Faraday Discussions

Cite this: *Faraday Discuss.*, 2018, **209**, 371



# Selectivity and polarization in water channel membranes: lessons learned from polymeric membranes and CNTs

Viatcheslav Freger *

Received 2nd March 2018, Accepted 26th March 2018
DOI: 10.1039/c8fd00054a

Water channels are employed by nature to move pure water across cell membranes while selectively rejecting salts. At present, synthetic channels successfully mimic water permeation, yet even the best channels, such as carbon nanotubes (CNTs) and graphene oxide stacks, still fall short of the selectivity target. The present paper analyzes factors that may help to enhance and control salt rejection based on the lessons learned from conventional membranes and CNTs. First, it highlights the importance of raising the ion self-energy (dielectric mechanism), which suggests that having the channels both narrow and surrounded by a low-dielectric environment is key to high selectivity. In contrast, pore charge alone is insufficient, yet it may help to enhance and tune ion rejection, provided that non-mean-field effects enhanced in low-dielectric pores, such as ion association and sorption, especially of $H^+$ and $OH^-$ ions, are properly understood and addressed in the channel design. Second, the role of concentration polarization (CP) is analyzed, which shows that the CP level is apparently low in isolated channels or microscopically small membranes. However, the geometry of the diffusion field should change and CP should increase drastically in macroscopic membranes incorporating densely spaced channel arrays. If not properly addressed in membrane design, the increased CP level in scaled-up channel-based membranes may significantly compromise the observed selectivity and require that target of selectivity be re-set to an even more challenging value. These points may help guide the future development of high-performance artificial water channels and their scale-up towards utilization in next-generation water purification membranes.

## 1. Introduction

Nature employs water channel proteins (aquaporins) to purify water to a high degree by rapidly shuttling it across the membranes as well as preventing ions from doing so. The high selectivity of water channels is due to the highly optimized chemistry, charge and geometry of the channels.[1] While biomimetic and synthetic

*Technion – Israel Institute of Technology, Wolfson Department of Chemical Engineering, Haifa, 32000, Israel. E-mail: vfreger@technion.ac.il*

channels mimic the permeation rates of water,[2–6] achieving the selectivity levels, commensurate with that of aquaporins in their native environment, seems far more challenging at present. For instance, the current state-of-the-art CNT porins[2,6–8] and graphene oxide channels[9] show salt rejection that barely exceeds 90% even for the best rejected divalent ions. The ultrahigh permeability may show diminishing benefits when increased much beyond the current level.[10] On the other hand, enhanced selectivity may offer a clear benefit for current technology.[11]

At present, it is clear that ion rejection consistently improves when the channel size is reduced.[2,6] Such results are commonly interpreted in a qualitative way by assuming that the size of the hydrated ion is the threshold pore size at which ion rejection becomes significant.[9,12] However, insights obtained by molecular dynamics (MD) simulations reveal physical mechanisms of transport and selectivity in channels and membranes that are more complex.[13–16] Unfortunately, it is not always straightforward to extrapolate conclusions from MD to real experimental conditions and settings, which often differ from those used in simulations. In this respect, simplified models and arguments that can still capture the underlying physics and transparently explain the observed trends might be of high value for quantifying the pore size effect and formulating practically useful criteria. In particular, such simple theories would also help to address the critical question of whether the desired level of ion rejection is achievable for realistic pore widths and in realistic designs and setups.

This paper will highlight lessons recently learned from studies of polymeric desalination membranes and CNT channels that may apply to water channels in general. One lesson is concerned with the mechanism of selectivity, which is mainly related to the exclusion of ions from the pore. In this respect, the paper will emphasize the role of the dielectric mechanism, which acts by increasing the self-energy of an ion in the channel, rather than its interaction with other charges.[17–20] This mechanism is strongly pore- and ion-size-dependent and may be easily mistaken for a steric effect, despite being distinctly different. It allows stronger and more robust ion exclusion than the commonly considered repulsion by charged groups located at the pore walls. The dielectric exclusion may however complicate the picture, by promoting non-trivial effects such as ion binding and association, which might both suppress and enhance salt permeation.

The second point highlighted in the paper is concerned with the effect of mass transfer limitations. This effect is associated with the solution adjacent to the membrane, collectively referred to as concentration polarization. We will show that, without properly considering this limitation, extrapolating the performance of individual channels to large channel arrays may significantly overestimate the performance. Ignoring such limitations may largely underestimate the challenges of developing macroscopic membranes based on artificial channels and, in particular, meeting the target selectivity.

## 2. The mechanisms of selectivity and ion exclusion

### 2.1. Diffusivity and sorption selectivity factors

Similarly to membranes,[21] the selectivity of a channel may be quantified as the selectivity factor defined as the ratio of the permeabilities to salt (s) and water (w).

 

$$\alpha_P = \frac{P_s}{P_w} = \frac{D_s}{D_w} \times \frac{\Gamma_s}{\Gamma_w} = \alpha_D \alpha_\Gamma \quad (1)$$

Here and below, the permeabilities $P_s$ and $P_w$ are not necessarily normalized to thickness and/or area, however, their ratio $\alpha_P$ is an intrinsic material property, since the geometry cancels out in eqn (1). Eqn (1) breaks $\alpha_P$ down to diffusive and sorption factors, defined as the corresponding ratios of the diffusion ($D$) and partitioning ($\Gamma$) coefficients of the permeant species. Note that, in the absence of a net electric current, salts will always permeate as neutral combinations of their constitutive ions, therefore, salt permeability will be derived from ion permeabilities and be limited by the least permeable ion of the salt.

The target value of the salt–water selectivity $\alpha_P$ of the water channels should be of the order $10^{-5}$, typical of today's reverse osmosis membranes (see Section 3). It seems unlikely that such a low value could be achieved through the diffusion factor $\alpha_D$, since the relevant radii of the permeant species are not sufficiently different. Admittedly, there is an uncertainty as to which type of radius, *e.g.*, hydrated or bare, would be most appropriate for assessing diffusivity in channels through the Stokes–Einstein relation. Moreover, the most appropriate radii may differ for different phenomena, *e.g.*, diffusion and sorption. Nevertheless, all types of radius for the most abundant inorganic ions, $Na^+$, $K^+$, $Ca^{2+}$, $Mg^{2+}$, $Cl^-$ and $SO_4^{2-}$, fall between 0.08 to 0.23 nm; the only exceptions being the Stokes radii of $Ca^{2+}$ (0.31 nm) and $Mg^{2+}$ (0.347 nm) in water.[21] Since the bare radii of $Ca^{2+}$ and $Mg^{2+}$ are under 0.11 nm, the large Stokes radii reflect strong hydration in water, however, in a channel it may not be as strong, therefore, the Stokes radii may be closer to the bare radii.

Furthermore, the size of a water molecule is similarly uncertain and may range from 0.1 nm, the Stokes radius deduced from water self-diffusion, to about 0.14 nm, the mean van der Waals radius deduced from electronic structures and interpolated crystallographic data for different oxygen-containing ions.[22,23] Then, when it comes to transport through water channels, all ion sizes are not that different from the size of a water molecule. Considering the similar size of ions and water and the fact that many artificial water channels are significantly larger, which is just as important, the diffusion selectivity factor is unlikely to be significant. Moreover, trying to enhance this factor by tightening the channels down to the size of the ions and water may compromise water permeability[13] and is probably not the right way to go.

Very low values of $\alpha_P$ are then more likely to be achieved *via* $\alpha_\Gamma$. Since water is supposed to fill channels, $\Gamma_w \sim 1$ and hence the sorption selectivity is to be controlled mainly by the salt (ion) partitioning. Ultimately, this sets $\Gamma_s$ as the key parameter. The next section briefly reviews the main mechanisms that control $\Gamma_s$ in synthetic membranes.

### 2.2. The three ion exclusion mechanisms

The concept of ion exclusion that is currently adopted in polymeric membranes considers three distinct physical mechanisms.[20,24–27] The first is steric exclusion, which is an entropic effect that is not unique to ions, whereby permeant molecules confined in a pore or free-volume cavity increasingly lose their freedom when the pore and permeant sizes become close. However, it is a relatively weak effect, unless the permeant species very closely fits the pores. For instance, the

Ferry model including translational entropy only[28] predicts that an already modest steric partitioning coefficient $\Phi = 0.1$ will require no more than 32% difference between the pore and solute radii. A good steric separation then requires that permeant species significantly differ in size and the pores be exceptionally rigid and uniform to sharply differentiate between the permeant species. This, just like a low $\alpha_D$ value, might be too difficult to achieve for water and ions.

The second mechanism is the Donnan exclusion, which arises from the interaction with fixed charged groups present in the membrane. The classical Donnan model considers an ideal solution of ions in the membrane and a smeared uniform mean-field Donnan potential, collectively imposed by the fixed charges on all ions to enforce the electroneutrality of the membrane phase. Such an idealized model ignores the screening of the fixed charges and thus overestimates the strength of charge exclusion, *i.e.*, for a given fixed charge density the actual $\Gamma_s$ value will always be higher than the $\Gamma_s$ value predicted by the ideal Donnan model.

In contrast to Donnan exclusion that considers inter-ionic interactions, the third mechanism, dielectric exclusion, originates from ion solvation in the medium, *i.e.*, ion self-energy $W$. This energy is always positive and large for non-polar low-dielectric media or nanopores in a low-dielectric matrix. The exclusion then follows from the positive self-energy difference $\Delta W$ between the membrane and solution phases.

One may write down a mean-field relation incorporating all three mechanisms, Steric, Donnan and-diElectric (SDE), and relate the $\Gamma_s$ value of the invading free salt (*i.e.*, co-ions) to the solution composition and membrane characteristics. For example, for a solution of a single monovalent salt (such as NaCl) of concentration $C_s$ and a membrane of fixed charge density $X$, the SDE relation will be as follows

$$\ln[\Gamma_s C_s(X + \Gamma_s C_s)] + \frac{\Delta W_s}{kT} = 2\ln[\Phi_s C_s], \tag{2}$$

where $\Phi_s = (\Phi_+\Phi_-)^{0.5}$ is the salt steric exclusion coefficient (the average of the cation and anion) and $\Delta W_s = \Delta W_+ + \Delta W_-$. When $X \gg \Gamma_s C_s$, *i.e.*, the membrane charge is large compared to the invading salt, an explicit solution of eqn (2) is

$$\Gamma_s \approx \frac{{\Phi_s}^2 C_s}{X} \exp\left(-\frac{\Delta W_s}{kT}\right). \tag{3}$$

Eqn (2) and (3) are easily generalized to multivalent salts and mixtures and may be used to relate salt exclusion to physical characteristics of the channel that determine parameters $X$ and $\Delta W_s$. They also indicate that salt partitioning is inherently concentration dependent.

We reiterate that the mean-field eqn (2) and (3) imply that all ions are subject to the same mean-field Donnan potential. This assumption may break down in many cases, *e.g.*, in channels that are wider than Debye length[29] or when ion non-ideality, *e.g.*, ion correlations[30] or association[24] (see Section 2.4), is significant. As a result, even for strongly charged pores, the dependence may deviate from the linear relation $\Gamma_s \propto C_s$ suggested by eqn (3). In such cases, the effective values of $X$ and $\Delta W_s$ will vary with $C_s$ as well. Nevertheless, eqn (2) and (3) may be useful

 

guiding relations, whenever the variation of $X$ and $\Delta W_s$ can be estimated or modelled, as elaborated next.

### 2.3. Relation of selectivity to physical characteristics

The classical Born equation[31] is commonly used to obtain realistic estimates of $W$ and connect it to the characteristics of the ion and medium. It ignores inter-ionic interactions and integrates the electrostatic energy density around a lone ion in an infinite dielectric continuum to yield

$$\frac{W_\pm}{kT} = \frac{{z_\pm}^2 e^2}{8\pi\varepsilon_0 \varepsilon r_\pm kT} \equiv \frac{1}{2}\frac{{z_\pm}^2 \lambda_B}{r_\pm} \equiv \frac{1}{T^*}, \quad (4)$$

where $z$ and $r$ are the charge (in units of electron charge $e$) and the radius of the ion, and $\varepsilon$ is the dielectric constant. The last two relations define the Bjerrum length $\lambda_B$ and reduced temperature $T^*$ of the medium. In water $\lambda_B \approx 0.7$ nm and $T^* \sim 1$ for most ions, but when $\varepsilon$ drops to 10, which corresponds to a mildly hydrophobic or moderately hydrated medium, $\lambda_B$ increases to 5 nm and $T^*$ becomes small ($T^* \ll 1$).

Experimentally measured $\Delta W$ for different ions in water relative to vacuum are best matched by so-called Born ion radii, which are only slightly larger than bare radii, but do not correlate as much with the corresponding Stokes radii.[32] The Born or bare radii then seem to be the most appropriate choice for calculating $W$ in low-$\varepsilon$ media. Given $r$ values are typically 0.1–0.2 nm, for $\varepsilon = 10$, the exponential factor in eqn (3) may be as small as $10^{-5}$ for monovalent ions and even $10^{-10}$ for divalent ions or for still lower dielectric constant. This may be compared with the effect of $X$, whose nominal values rarely exceed 1 M in membranes.[33] Even when $C_s$ is as low as 10 mM, the Donnan exclusion factor $C_s/X$ will only be about $10^{-2}$, which is clearly insufficient to reach the aforementioned target of selectivity.

This simple argument emphasizes that the reliance on fixed charges alone is insufficient and it is critical to employ the dielectric mechanism as well. The latter can not only work on its own, as it does in the case of cellulosic membranes,[18] but can also enhance the other mechanisms, as eqn (3) emphasizes. Incidentally, that may be the case for in aquaporin channels as well, since the low-dielectric material that surrounds the charged constriction should raise the energy of charge repulsion.

In water-filled channels or nanopores, even for a lone ion, the situation becomes more complex. The simple Born equation is not valid any more, since the polarization of the pore-matrix interface by the ion (*cf.* image charges) modifies the self-energy in a strongly pore geometry-dependent manner.[17,18,30,34–36] Yaroshchuk[20] reviewed the problem, giving expressions for pores of different geometries, including charged pores. In general, compared with a non-porous matrix, $W$ is reduced in a pore by a term that is inversely proportional to the pore size for a given pore geometry. The dielectric exclusion then rapidly weakens with increasing pore size, which may be readily misinterpreted as a signature of steric exclusion.

The above analysis indicates that best recipe for creating a highly selective channel is to make the pore as small as possible and ensure the pore environment is as low-dielectric as possible. For instance, the relatively slow $r^{-2}$ decay of the electrostatic energy density around an ion implied in the derivation of (4) suggests

that, as well as pore walls, fairly distant pore surroundings may have some effect on ion exclusion. Obviously, tuning dielectric properties, *i.e.*, the hydrophobicity/hydrophilicity of the pore, requires some care, since a hydrophobic pore may eventually become impermeable to water. The channel should then be as narrow and hydrophobic as possible yet still allow fast water permeation.

On the other hand, tuning channel charge alone is insufficient for having a high selectivity, even though it may enhance and tune salt rejection and perhaps help keep the pore water-permeable too. However, keeping a significant pore charge in a low-dielectric environment may not be straightforward, since much of the charge may become associated and inactive, as explained in the next section.

### 2.4. Ion association

Apart from non-trivial relations to pore geometry, another complex aspect of dielectric exclusion is its intimate relationship with the effects responsible for strong deviations from mean-field, in particular, ion sorption and association. Such effects, which invalidate the mean-field approach, are controlled essentially by the same parameters as the self-energy, namely, the charge and size of the ions and the dielectric constant of the medium, or, concisely, by $T^*$. The consequences are most dramatic in charged low dielectric media, *i.e.*, exactly in the conditions desired for maximal selectivity.

To illustrate the point, we may adopt the same idea as in the derivation of eqn (4) and consider hard-ball ions of the same size and absolute charge in a dielectric continuum. In this model, known as a restrictive primitive model (RPM), the association constant for ion pairs is[37]

$$K \cong 4\pi b^3 T^* \exp\frac{1}{T^*}, \tag{5}$$

where $b = r_+ + r_- = 2r$ is the distance of closest approach in the pair. The low-dielectric conditions correspond to $T^* \ll 1$, in which case the missing numerical factor in eqn (5) is close to 1.[37]

For simplicity, let us neglect the small self-energy in water and steric exclusion, *i.e.*, assume that $\Delta W_s/kT \approx 2/T^*$ and $\Phi_s \approx 1$. Without fixed charge ($X = 0$), eqn (2) yields

$$\Gamma_s = \Gamma_\pm \cong \exp\left(-\frac{1}{T^*}\right) \ll 1, \tag{6}$$

which means that for $T^* \ll 1$ the ion concentration in the membrane $\Gamma_s C_s$ will be low. The fraction of associated ions is given by

$$\frac{K(\Gamma_s C_s)^2}{\Gamma_s C_s} = K\Gamma_s C_s \cong C_s b^3 T^* \ll 1. \tag{7}$$

This means that in a non-charged low-dielectric membrane the small fraction of ion pairs will be small and contribute negligibly to salt transport, as was established long ago for lipid membranes.[36]

However, if the membrane contains a large fixed charge $X$, it will also have to contain an equivalent concentration of counter-ions, a substantial fraction of which may associate. Roughly, this will happen when the Bjerrum length $\lambda_B$ exceeds the spacing of ionic groups, thus electrostatics start dominating over

 

thermal motion. A certain similarity may be seen with the well-known Manning counter-ion condensation on linear charges (polyelectrolytes),[38] however, the analogy is superficial, since the parameters controlling the residual effective charge are different.

For the present case of discrete fixed charges dispersed in 3D space, consider the relationship between the residual fixed charge density $X_{ef}$ and the total fixed charge $X$. Since the concentration of free non-associated counter-ions has to be $X_{ef}$ as well, the association equilibrium reads

$$X_{ef} = \frac{X}{1 + KX_{ef}}. \tag{8}$$

If the association constant is small, $KX_{ef} \approx KX \ll 1$, the effective charge is not that much different from the total one $X_{ef} \approx X$. However, if the association constant is large, $KX_{ef} \approx KX \ll 1$, eqn (8) becomes

$$X_{ef} \approx \frac{X}{KX_{ef}}, \tag{9}$$

where the effective fraction of the fixed charge is approximately

$$\frac{X_{ef}}{X} \approx (XK)^{-1/2} \cong \left(Xb^3\right)^{-1/2} T^{*-1/2} \exp\left(-\frac{1}{2T^*}\right). \tag{10}$$

This indeed becomes small, when $T^*$ is small enough.

The resulting $X_{ef}$ then replaces $X$ in eqn (3), which shows that salt partitioning is affected by $T^*$ in two ways, through $X_{ef}$ and $W_s$. Ultimately, this yields a weaker exclusion, with a more complex dependence on $T^*$ and a weaker dependence on the nominal fixed charge $X$ than eqn (2), as follows

$$\Gamma_s \approx \frac{C_s}{X_{ef}} \exp\left(-\frac{2}{T^*}\right) \approx \frac{C_s b^{3/2}}{X^{1/2}} T^{*1/2} \exp\left(-\frac{3}{2T^*}\right). \tag{11}$$

The last four relations imply that the mean-field (Donnan) potential still apples to non-associated ions, in the spirit of Bjerrum's treatment of ion association.[39] However, it does not apply to associated ions any more, since mean-field cannot adequately describe strong and rapidly varying potential around fixed charges, leading to strong spatial correlations between the fixed charges and counter-ions and their immobilization.

Deviations from mean-field, implied in Donnan or Poisson–Boltzmann models, are usually only significant in aqueous solutions for multivalent ions.[40] They manifest themselves in effects such as surface charge reversal or layering, which can be viewed as weak forms of association and require introducing non-field elements in the models.[34,40–42] Here we see that in highly selective membranes such effects can be strong even for monovalent ions, as our recent MD simulations of polyamide membranes demonstrate.[15] For this reason, in order not to overestimate ion exclusion, the Poisson–Boltzmann description that has been widely used for modelling charged nanochannels[29,42–44] must be modified for narrow and highly selective water channels that employ low-$T^*$ regimes. Incorporation of association equilibria into such models as a way to calculate an

effective charge might offer a simple phenomenological way to address such deviations.

### 2.5. Specific ion sorption in polymers and nanotubes

**2.5.1. Polymeric membranes.** The previous section highlights the role and importance of ion association in low-$T^*$ membranes and nanochannels. However, strong ion-specific interactions, which are absent in an RPM but present in real systems, can substantially modify the ion exclusion relation even at moderate $T^*$. Ions that may be particularly prone to such behaviour are $H^+$ and $OH^-$, which are inherently present in any aqueous system. Apart from being uniquely small, which facilitates association, these ions may readily form hydrogen bonds and even covalent bonds with many chemical groups and water within membranes or channels. A well-known example is the binding of $H^+$ by weakly acidic carboxyl groups. Due to covalent bonding, its association constant in water is $10^4\ M^{-1}$ ($pK_a \sim 4$), which is many orders of magnitude stronger than purely electrostatic association. In desalination membranes the $pK_a$ values of carboxyl groups were shown to shift several orders of magnitude up to ~8–9.[45] The extra self-energy of the fixed carboxyl charges $W \sim 10\ kT$ removed upon protonation explains this shift. Eqn (4) with appropriate values of $r$ and $\lambda_B$ agrees well with this $W$ value.

Recent studies demonstrate that specific ion binding or sorption may not even require a large $X$ value and may be remarkably strong even in nominally neutral low-$T^*$ materials lacking any acidic or basic binding sites. This is most readily revealed by analysing the membrane conductance. Indeed, the specific conductance ($\Lambda$) of a polymer equilibrated with an ionic solution is directly connected to ion permeabilities and, ultimately, to ion diffusivities and partitioning, as follows[46]

$$\Lambda = \frac{F^2}{RT}\sum_i P_i C_i z_i^2 = \frac{F^2}{RT}\sum_i D_i \Gamma_i C_i z_i^2, \tag{12}$$

where the summation is for all ions in solutions and the $P$'s are area- and thickness-normalized. Unlike the salt permeabilities determined by the least-permeating ion of the salt, $\Lambda$ is controlled by the fastest permeating ion, offering complementary insight into ion permeation.

Our recent results on the ion conductance of polyamide membranes and Nomex films, which are known to have a high water–salt selectivity, reveals strong affinity effects.[24,47] The conductance of Nomex films immersed in solutions of different chloride salts, covering a 3 orders of magnitude $C_s$ range, showed an unusual 1/2-power scaling of conductivity[24,47]

$$\Lambda \propto C_s^{1/2}, \tag{13}$$

Curiously, the measured dependence was virtually independent of cation type, except for HCl solutions that showed the regular linear scaling $\Lambda \propto C_s$. The conductivity for salts was also pH-dependent, increasing by about an order of magnitude when the pH dropped by 2 units. This strongly suggests that, despite the very low $H^+$ concentration in solution, the neutral combination that the polymer uptakes is always HCl and not metal salts MCl or $MCl_2$, thereby one has

$$\Gamma_{M^+}C_{M^+} \ll \Gamma_{H^+}C_{H^+} \approx \Gamma_{Cl^-}C_{Cl^-} \propto (C_{H^+}C_{Cl^-})^{1/2} = 10^{-pH/2}C_s^{1/2}, \tag{14}$$

in agreement with eqn (13). Such a behavior then indicates an exceptionally high affinity of Nomex to protons. The crossover to $\Lambda \propto C_s$ at high $C_s$ lets us estimate that proton affinity to polyamide was about $10^3$ times that of $Na^+$ and $>10^7$ times that of $Ca^+$, which is far beyond simple electrostatics. Presumably, the reason for such exceptional affinities is, on one hand, the strong dielectric exclusion of salt cations and, on the other hand, strong and specific proton–polymer interactions.

The effect of $H^+$ uptake is equivalent to the formation of a positive effective "fixed" charge $X_{ef}$. However, due to the need to take up an equivalent amount of anions and compete with other cations, the charge is not "fixed" and depends on both pH and $C_s$. Formation of such positive charge may have a significant impact on both permselectivity and salt permeation. An increase in positive charge will always facilitate anion permeation and hold back cations. The ultimate effect will then depend on which ion controls salt permeation. For instance, if the membrane is inherently more permeable to anions than cations, proton uptake (lower pH) will increase salt permeability, yet it will do the opposite if the membrane is preferentially permeable to cations.[24,48]

**2.5.2. Carbon nanotube channels.** A behaviour that resembles that of Nomex was reported for the conductivity of CNT nanochannels, however, the interpretation brought up much controversy. For wider nanotubes, where screening effects come into play, Secchi *et al.* proposed a model that predicts an unusual scaling of $\Lambda \propto C_s^{1/3}$ that seemed to conform to their data.[44] The proposed mechanism assumed that the charge-generating mechanism in CNTs was the specific adsorption of $OH^-$ ions, which rendered the channel negatively charged. The model was, however, criticized by Biesheuvel and Bazant,[29] who pointed out that it relied on two physically incompatible assumptions. Instead, they proposed an *ad hoc* Langmuir-type OH adsorption, thus the trend observed by Secchi *et al.* was interpreted as a transition between adsorbed charge saturation regime $\Lambda \propto C_s^0$ and linear high-salt regime $\Lambda \propto C_s^1$.

Curiously, Biesheuvel and Bazant also pointed out a possibility of $C_s^{1/2}$ scaling at unattainably low $C_s$. Nevertheless, such scaling was reported for $C_s$ values ranging from <0.01 M to >1 M by Tunuguntla *et al.*[6] for short (~12 nm) 0.8 nm CNTs, as well as by Amiri *et al.*[2] for 20 μm-long 1.5 nm CNTs. These authors attributed the observed scaling to progressively screened carboxyl charges at the nanopore rims. This conclusion was based on the drop in conductance and transition to regular $C_s^1$ scaling below pH 5, which is close to the $pK_a$ of carboxyl groups. Yet, it is surprising that the effect of rim charges, which is supposed to extend over a few nanometers and is thus likely for short CNTs used by Tunuguntla *et al.*, could control the transport in much longer CNTs in experiments by Amiri *et al.* as well. Besides, maintaining $C_s^{1/2}$ scaling without saturation over such a wide $C_s$ range is less likely for genuine fixed charges (carboxyls) at the rim that directly faces an aqueous environment.

This controversy will have to be resolved in the future, but it may be noted that the above data and other results discussed in these reports might be well explained by the competitive adsorption of $OH^-$ on CNT walls. This should be aided by the strong dielectric exclusion of salt cations, in a manner similar to $H^+$ uptake in Nomex. For instance, the crossover at pH ~ 5 could simply correspond to the isoelectric point (pI), at which the large affinity of CNT walls to $OH^-$ no longer compensates for the drop in $OH^-$ concentration and thus $H^+$ and/or salt

take over. Note that a similar pI is often observed for many uncharged hydrophobic surfaces in water.[49]

The results for CNTs therefore indicates that, just as in polymeric membranes, charge control in highly selective (*i.e.*, strongly salt- and ion-excluding) channels, is likely to encounter a specific adsorption of $H^+$ and $OH^-$ ions. This may modify the channel selectivity in a complex way that may depend on the channel chemistry, solution composition and pH.

As a final note, the reported transport data for 0.8 nm CNTs[6] mean that the estimation of the level of water-ion selectivity is achievable today in CNT channels. At conditions roughly matching those of seawater, 0.5 M KCl and pH 7.5, 0.8 nm CNTs showed a conductance $G$ of $\sim$ 50 pS and $K^+/Cl^-$ selectivity of $\sim$ 200 : 1. This translates to the channel permeability to KCl, controlled by chloride, as follows

$$\frac{GRT}{200F^2C_s} = \frac{50\times10^{-12}\times2.5\times10^3}{200\times(10^5)^2\times0.5\times10^3} \approx 10^{-22}\ \text{m}^3\ \text{per s per channel.}$$

On the other hand, the osmotic water permeability, measured using a stop-flow technique for the same CNTs at 0.6 M NaCl and pH 7.8 was found to be about $P_w \sim 10^{-18}$ m$^3$ per s per channel. That yields a selectivity factor $\alpha_P$ of $\sim 10^{-4}$, which misses by just an order of magnitude the $10^{-5}$ target set by today's commercial desalination membranes. Since 0.8 nm tubes are still not the narrowest possible, this result should be seen as encouraging, provided the challenge of concentration polarization, analysed in the next section, is addressed.

# 3. Concentration polarization: the case of water channels

## 3.1. Polarization relations for planar membranes

Concentration polarization (CP) refers to the mass transfer resistances associated with unstirred solution layers adjacent to a selective membrane, turning the membrane into an inferior "multilayer". Its impact is nearly always detrimental and undesired and is two-fold. First, the added resistance slows-down the permeation rates. Second, the solution layer, which lacks selectivity, reduces the overall selectivity of the "multilayer".

A major limitation for the overall permeation rate (flux or current) is set by the diffusion permeability of the unstirred boundary layer $D/\delta$, commonly called the boundary layer mass transfer coefficient, where $\delta$ is the boundary layer thickness and $D$ is the relevant diffusivity. For macroscopic membranes, hydrodynamic conditions largely determine $\delta$ and reducing it below 10 μm requires high-shear flows, which weighs excessively on the energy consumption. As a result, $\delta$ is normally in the range 10–50 μm thereby $D/\delta$ rarely exceeds 20–30 μm s$^{-1}$. An attempt to increase water flux or ion current beyond this rate by increasing the driving force, *e.g.*, pressure or electric potential, will result in a loss of most driving force within the unstirred layer. This general argument applies to all membrane processes, however, the effect on permeation and selectivity and the parameters controlling CP may somewhat differ, depending on the specific process.

In osmotic processes, it is customary to use water and salt permeability coefficients $A$ and $B$ related to permeabilities $P_w$ and $P_s$ defined per unit membrane area, as follows[50]

$$A = \frac{P_w V_w}{RT}, \quad B = P_s, \tag{15}$$

where $V_w$ is the water molar volume. Typical values for modern reverse osmosis (RO) membranes are of the order $A \sim 1$ μm s$^{-1}$ bar$^{-1}$ and $B \sim 10^{-2}$ μm s$^{-1}$, which is what sets the target value for the selectivity $\alpha_p$ at $\sim 10^{-5}$. In RO, the water volume flux $J_w$ may be viewed as an independent operational variable controlled by the applied pressure $\Delta P_{net}$ (applied pressure minus osmotic pressure difference), $J_w = A\Delta P_{net}$. To obtain the steady-state salt flux $J_s$ for a given $J_w$, salt permeation through the membrane has to match convection-diffusion in the upstream boundary layer. For regular planar membranes, only the dimension normal to the membrane surface ($x$) needs to be considered, as follows[21]

$$J_s = B(C_m - C_p) = -D_s \frac{dC}{dx} + J_w C, \tag{16}$$

where $C_m$ is the concentration at the feed-membrane interface and $C_p = J_s/J_w$ is the permeate concentration. Solution of eqn (16) shows that the observed salt permeability will be larger than the "ideal" permeability $B$,

$$B_{obs} = B \exp\left(\frac{\delta}{D_s} J_w\right), \tag{17}$$

This is a result of the exponential growth of $C_m$, which will also increase the osmotic difference and prevent the increase of $J_w$ to much beyond the diffusion permeability of the boundary layer $D_s/\delta$, when the applied pressure increases.

The situation is different in forward osmosis (FO), where the same salt concentration difference between brine (b) and diluate (d) drives both water and salt in opposite directions.[51] As a result, the virtual "permeate" concentration $C'_p = J_s/J_w = B/ART$ is fixed by the ratio of permeabilities $B/A$, regardless of CP. However, CP will greatly affect the fluxes. Coupling the convection–diffusion in two unstirred layers on b and d sides with permeation through the membrane yields an implicit relation for $J_w$

$$J_w = ART\left\{\left(C_b + C'_p\right)e^{-\frac{\delta_b}{D}J_w} - \left(C_d + C'_p\right)e^{\frac{\delta_d}{D}J_w}\right\}. \tag{18}$$

Solution of eqn (18), illustrated in Fig. 1, shows that (a) CP reduces the osmotic driving force below the ideal value $C_b - C_d$, and (b) there is an upper limit for achievable water flux, determined by the combined diffusion resistance of both unstirred layers and membrane selectivity ($C'_p$), as follows

$$J_{w,lim} = \frac{D}{\delta_b + \delta_d} \ln\frac{C_b + C'_p}{C_d + C'_p}. \tag{19}$$

Note that $\delta_b$ or $\delta_d$ may contain the resistance of porous supporting layers from the membrane as well ("structure factor"[51]).

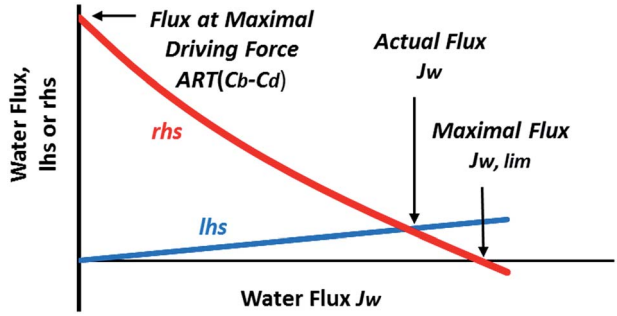


Fig. 1 Graphical solution of eqn (18): the blue and red lines represent the left- and right-hand sides of eqn (18); their intersect gives the actual flux under given CP conditions. The intersect of the rhs line and the *y*-axis corresponds to the flux at negligible CP, where the entire driving force falls on the membrane. The intersect of the rhs line and the *x*-axis corresponds to the limiting flux given by eqn (19), where membrane permeability $A$ is infinitely large.

Finally, consider an electric current through an ion-selective membrane surrounded by a (monovalent) salt solution of concentration $C_s$ and diffusivity $D_s$. At one side, the membrane–solution interface will get progressively depleted of salt and the potential drop will exponentially increase when current density approaches the limiting density, given by[52]

$$i_{\lim} = \frac{FD_sC_s}{\delta(t_m - t_s)}, \tag{20}$$

where $t_m$ and $t_s$ are the counter-ion transference numbers for the membrane and solution. Here the relevant diffusion resistance $\delta(t_m - t_s)/D_s$ limits the rate of supply of co-ions to the membrane surface, which is necessary to prevent the infinite increase of the potential drop.

The above limitations imposed by CP have been well recognized as critical for conventional planar membranes. They may, however, change significantly for water channels. This aspect may be particularly critical for scale-up from individual channels or pore-spanning membrane patches or vesicles of microscopic size to macroscopic channel arrays, which may result in a drastic change in CP conditions, as discussed in the next section.

### 3.2. Channels and channel-array membranes

**3.2.1. Polarization in an isolated channel.** Electrochemists were perhaps the first to recognize the phenomenon of polarization, which bears much similarity between solid electrodes and perm-selective membranes. They also came up with a way to reduce polarization and decouple it from hydrodynamics by using microelectrodes of lateral dimensions that are much smaller than the unstirred layer thickness $\delta$.[53]

Nanoscopic channels embedded in an impermeable membrane, *e.g.*, a lipid bilayer, are analogues of microelectrodes, as much as conventional membranes are analogues of planar electrodes. What makes the major difference between a channel and a macroscopic membrane is the fact that a semispherical diffusion field centered at the channel mouth will replace the planar boundary layer (*cf.*

Fig. 2a and b). As a result, for RO, the radial coordinate $r$ and flow rates $Q$ will replace coordinate $x$ and fluxes $J$ in eqn (1) to yield[54]

$$Q_s = P_s(C_m - C_p) \approx -2\pi r^2 D_s \frac{dC}{dr} + Q_w C. \quad (21)$$

Note that, from here on, $P_w$ and $P_s$ are redefined per channel. Solving eqn (21) replaces eqn (17) with

$$P_{s,obs} \approx P_s \exp\left(\frac{Q_w}{2\pi D_s R_c}\right), \quad (22)$$

where $R_c$ is the channel radius, which is assumed to be much smaller than the outer radius $R_o$ of the diffusion profile, *i.e.*, the "thickness" of the diffusion profile in Fig. 2b, at which $C$ equals the bulk concentration $C_b$. Similar to $\delta$, the value of $R_o$ is determined by hydrodynamic mixing conditions, $R_o \sim \delta$. However, since $\delta \gg R_c$, hydrodynamics has essentially no effect on the observed permeability for a single channel.

For FO, eqn (18) and (19) are similarly replaced with relations

$$Q_w \approx P_w V_w \{(C_b + C'_p)e^{-Q_w/2\pi D_s R_c} - (C_d + C'_p)e^{Q_w/2\pi D_s R_c}\}, \quad (23)$$

$$Q_{w,lim} = \pi D_s R_c \ln \frac{C_b + C'_p}{C_d + C'_p}. \quad (24)$$

Finally, the limiting current $I_{lim}$ for an ion-selective microchannel will be

$$I_{lim} \approx \frac{2\pi R_c F D_s C_s}{t_m - t_s}. \quad (25)$$

The limitations set by eqn (22), (24) and (25) are significantly less restrictive than for their planar membrane counterparts eqn (17), (19) and (20). The

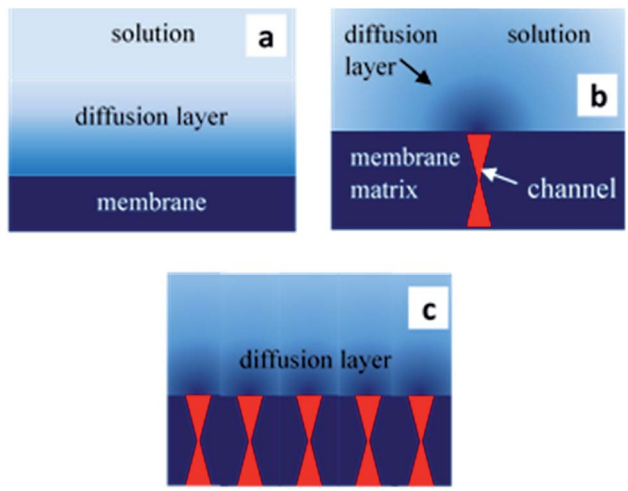


Fig. 2 Concentration polarization and the geometry of the diffusion field in solution adjacent to (a) a planar homogeneous membrane, (b) an isolated single channel and (c) a closely spaced channel array with overlapping diffusion layers.

aforementioned data presented by Tunuguntla *et al.* on 0.8 nm CNT channels ($R_c = 0.34$ nm)[6] may be used to illustrate the point. For the reported permeability $P_w \sim 10^{-18}$ m$^3$ per s per channel, even if one takes the osmolarity difference $C_s$ as high as 1 M to maximize $Q_s$, the term under exponents in eqn (23) will be

$$\frac{Q_w}{2\pi R_c D_s} = \frac{P_w V_w C_s}{2\pi R_c D_s} \sim \frac{10^{-18} \times 1.8 \times 10^{-5} \times 10^3}{2\pi \times 0.34 \times 10^{-9} \times 1.5 \times 10^{-9}} \approx 0.006,$$

which indicates a negligible CP.

Similarly, the maximal current employed in potential reversal experiments with $C_s = 1$ M at the dilute solution side was of the order 10 pA, whereas eqn (25) estimates the limiting current as

$$I_{lim} \sim \frac{2\pi \times 0.4 \times 10^{-9} \times 10^5 \times 1.5 \times 10^{-9} \times 10^3}{1 - 0.5} \approx 2 \times 10^{-9} \text{ A} \approx 2 \text{ nA},$$

*i.e.*, three orders of magnitude larger, indicating a negligible effect of polarization on the measurements.

**3.2.2. Channel arrays: vesicles, nanopores, and macroscopic membranes.** In foreseeable implementation scenarios, scaled-up devices will require arrays of channels embedded in a macroscopically large membrane. Unfortunately, the negligible effect of polarization on isolated individual channels, highlighted in the previous section, may no longer apply to such arrays. The spherical symmetry of the diffusion fields around individual channels will transition to the regular planar one, once the fields of neighboring channels begin to overlap within the unstirred layer (Fig. 2c). The limiting flux or current is then anticipated to drop substantially already when $L \sim \delta$, where $L$ designates the average spacing of the channels. The analysis of the microelectrode arrays indicates that the behavior of an array will be indistinguishable from a planar membrane for $L < \delta/3$.[53]

The water flux per total footprint area of a channel array is related to the permeation rate per channel as

$$J_w = Q_w L^{-2}. \tag{26}$$

The need to maximize the flux is an incentive to minimize $L$, *i.e.*, increase the channel density. However, once $L$ in an array drops under $\delta$, the limiting values of flux or current per channel will also drop relative to an individual channel by a factor, *cf.* eqn (19), (24) and (26),

$$\frac{Q_{w,lim} L^2}{J_{w,lim}} \cong \frac{L^2}{\delta R_c}. \tag{27}$$

This factor can still make no difference for arrays inserted in membranes of microscopic area, such as vesicles employed in stop-flow experiments or membrane patches spanning a single nanopore for membrane potential and current measurements.[6] In such cases the planar diffusion field at distances less than the membrane size will transition to semi-spherical at larger distances. This means that the effective boundary layer thickness in such cases will correspond to the radius of the vesicle or nanopore membrane $R_m$, typically ranging from 50 to 1000 nm.

As an example, take $L \sim 10^{-8}$ m (10 nm), corresponding to a maximal density of aquaporins in living cell membranes,[55] which is obviously much smaller than the

membrane size $R_m$. Packing 1 nm channels ($R_c = 5 \times 10^{-10}$ m) in a vesicle even as large as $R_m \sim 5 \times 10^{-7}$ m (500 nm, typical of many living cells) yields

$$\frac{L^2}{R_m R_c} \sim \left(10^{-8}\right)^2 \Big/ \left(5 \times 10^{-7} \times 5 \times 10^{-10}\right) \sim 0.4.$$

This is an insignificant factor therefore CP is nearly as negligible as in a single channel. Channels in vesicles or nanopores then negligibly interfere with each other, as aquaporins apparently do in living cells, and are subject to negligible CP. Importantly, since $R_m \ll \delta$, hydrodynamics have no or little effect on CP.

However, in a macroscopic planar array of such density, an opposite relation $R_m \gg \delta$ holds, therefore the flow-dependent unstirred layer thickness $\delta \geq 10^{-5}$ m (10 μm) rather than membrane size will determine the limiting rate. The latter will then drop, relative to a single channel, by a factor

$$L^2/\delta R_c \leq (10^{-8})^2/(10^{-5} \times 5 \times 10^{-10}) \sim 0.02.$$

This >50-fold drop in limiting flux $J_{lim}$ may increase CP to an extent that the selectivity estimated for an isolated channel may be impossible to achieve in a membrane for any reasonable value of $J_w$.

As another example, consider the density of CNT porins used by Tunungutla *et al.*, which was 5–30 channels per 200 nm vesicle,[6] corresponding to $L \sim 10^{-7}$ m (100 nm). For this value and $\delta \sim 10$ μm and $L^2/\delta R_c \sim 1$, *i.e.*, packing channels in a planar array of such density will not make a difference in CP compared with an isolated channel. However, such a low-density array had a fairly low water permeability

$$A = \frac{P_w V_w}{L^2 RT} = \frac{10^{-18} \times 1.8 \times 10^{-5}}{(10^{-7})^2 \times 2.5 \times 10^3} < 10^{-12} \ \mathrm{m^{-1}\ s^{-1}\ Pa^{-1}},$$

which is too small, compared with today's RO membranes, $A \sim 5 \times 10^{-12}$ m s$^{-1}$ Pa$^{-1}$. An attempt to increase density to match this $A$ will reduce $J_{lim}$ by the same factor and exponentially increase CP.

Apparently, the problem of CP in macroscopic channel array membranes have no easy solution. The present analysis suggests that a careful optimization of the channel density may be required, still subject to fundamental upper limitation. When osmotic pressure is not large, *e.g.*, in purification of low-salinity feeds, very high channel selectivity may compensate for CP-enhanced salt permeation and allow some increase in water permeation rates. This re-emphasizes the importance of maximizing the channel selectivity.[11] In either case, the current polymeric membranes remain tough competitors for artificial channels, in terms of both selectivity and permeability.[56]

# 4. Conclusions

In foreseeable applications, the selectivity of artificial water channels may be as important as water permeability, yet at present, it is about an order of magnitude off the target set by today's polymeric membranes. The lessons learned from conventional membranes suggest that the dielectric mechanism is the one that is

most likely to deliver the desired selectivity. To achieve the required effect, it is equally crucial to have the channels both narrow and surrounded by a low-dielectric environment in order to raise the ion self-energy. In contrast, pore charge is apparently insufficient on its own to reach the required strength of exclusion. However, charges may help to enhance and tune ion rejection, provided non-mean-field effects, such as ion sorption and association enhanced in low-dielectric pores, especially of $H^+$ and $OH^-$ ions, are properly understood and addressed. As discussed here, such effects may significantly modify the pore charge and thus increase or decrease selectivity.

Another important point, well recognized in membrane science and analyzed here in the context of water channels, is the effect of concentration polarization. The presented analysis shows that the CP level is apparently always low in experiments with individual channels or microscopically small membranes. However, the situation may drastically change in macroscopic membranes incorporating densely spaced channel arrays, due to a different geometry of the diffusion field. As a result, projections from microscopic experiments to macroscopic membranes runs the risk of overestimating their potential performance. If not properly addressed in membrane design, the increased CP level in scaled-up channel-based membranes may significantly compromise the observed selectivity and require that the target of selectivity be re-set to an even more challenging level.

The points highlighted in this paper may help guide the future development of high-performance artificial water channels and their scale-up towards utilization in next-generation desalination and water purification membranes.

## Conflicts of interest

The author declares no conflicts of interests.

## Acknowledgements

The financial support by the Israel Science Foundation (grant #1152/11) and by a joint grant 2016627 from the United States-Israel Binational Science Foundation (BSF, Jerusalem, Israel), and the United States National Science Foundation (NSF) is acknowledged. The author thanks Dr Aleksandr Noy (LLNL and UC Merced) and Prof. Meni Wanunu (Northeastern U) for many illuminating discussions and for sharing data prior to publication.

## References

1 P. Agre, *Proc. Am. Thorac. Soc.*, 2006, **3**, 5–13.
2 H. Amiri, K. L. Shepard, C. Nuckolls and R. l. Hernández Sánchez, *Nano Lett.*, 2017, **17**, 1204–1211.
3 M. Barboiu, *Angew. Chem., Int. Ed.*, 2012, **51**, 11674–11676.
4 Y.-x. Shen, P. O. Saboe, I. T. Sines, M. Erbakan and M. Kumar, *J. Membr. Sci.*, 2014, **454**, 359–381.
5 Y.-x. Shen, W. Si, M. Erbakan, K. Decker, R. De Zorzi, P. O. Saboe, Y. J. Kang, S. Majd, P. J. Butler, T. Walz, A. Aksimentiev, J.-l. Hou and M. Kumar, *Proc. Natl. Acad. Sci. U. S. A.*, 2015, **112**, 9810–9815.

 

6 R. H. Tunuguntla, R. Y. Henley, Y.-C. Yao, T. A. Pham, M. Wanunu and A. Noy, *Science*, 2017, **357**, 792.
7 B. J. Hinds, N. Chopra, T. Rantell, R. Andrews, V. Gavalas and L. G. Bachas, *Science*, 2004, **303**, 62–65.
8 J. K. Holt, H. G. Park, Y. Wang, M. Stadermann, A. B. Artyukhin, C. P. Grigoropoulos, A. Noy and O. Bakajin, *Science*, 2006, **312**, 1034–1037.
9 J. Abraham, K. S. Vasu, C. D. Williams, K. Gopinadhan, Y. Su, C. T. Cherian, J. Dix, E. Prestat, S. J. Haigh and I. V. Grigorieva, *Nat. Nanotechnol.*, 2017, **12**, 546–550.
10 D. Cohen-Tanugi and J. C. Grossman, *Nano Lett.*, 2012, **12**, 3602–3608.
11 J. R. Werber, A. Deshmukh and M. Elimelech, *Environ. Sci. Technol. Lett.*, 2016, **3**, 112–120.
12 F. Fornasiero, H.-G. Park, J. K. Holt, M. Stadermann, C. Grigoropoulos, A. Noy and O. Bakajin, *Proc. Natl. Acad. Sci. U. S. A.*, 2008, **105**, 17250–17255.
13 B. Corry, *Energy Environ. Sci.*, 2011, **4**, 751–759.
14 M. Ding, A. Szymczyk, F. Goujon, A. Soldera and A. Ghoufi, *J. Membr. Sci.*, 2014, **458**, 236–244.
15 V. Kolev and V. Freger, *J. Phys. Chem. B*, 2015, **119**, 14168–14179.
16 Y. Luo, E. Harder, R. S. Faibish and B. Roux, *J. Membr. Sci.*, 2011, **384**, 1–9.
17 L. Dresner, *Desalination*, 1974, **15**, 371–374.
18 E. Glueckauf, *Desalination*, 1976, **18**, 155–173.
19 A. Szymczyk, N. Fatin-Rouge, P. Fievet, C. Ramseyer and A. Vidonne, *J. Membr. Sci.*, 2007, **287**, 102–110.
20 A. E. Yaroshchuk, *Adv. Colloid Interface Sci.*, 2000, **85**, 193–230.
21 M. H. V. Mulder, *Basic Principles of Membrane Technology*, Kluwer Academic, Dordrecht, The Netherlands, 1996.
22 M. Chaplin, Water Molecule Structure, http://www1.lsbu.ac.uk/water/water_molecule.html#g, accessed March 1, 2018.
23 F. Franks, *Water: a matrix of life*, Royal Society of Chemistry, 2007.
24 N. Fridman-Bishop, K. A. Tankus and V. Freger, *J. Membr. Sci.*, 2018, **548**, 449–458.
25 Y. Lanteri, P. Fievet and A. Szymczyk, *J. Colloid Interface Sci.*, 2009, **331**, 148–155.
26 S. Levchenko and V. Freger, *Environ. Sci. Technol. Lett.*, 2016, **3**, 339–343.
27 A. E. Yaroshchuk, *Sep. Purif. Technol.*, 2001, **22–23**, 143–158.
28 J. Giddings, *J. Phys. Chem.*, 1968, **72**, 4397.
29 P. Biesheuvel and M. Bazant, arXiv preprint arXiv:1610.01309, 2016.
30 S. Buyukdagli, M. Manghi and J. Palmeri, *Phys. Rev. Lett.*, 2010, **105**, 158103.
31 M. Born, *J. Phys.*, 1920, **1**, 45–48.
32 C. S. Babu and C. Lim, *Chem. Phys. Lett.*, 1999, **310**, 225–228.
33 L. A. Perry and O. Coronell, *J. Membr. Sci.*, 2013, **429**, 23–33.
34 S. Buyukdagli, M. Manghi and J. Palmeri, *J. Chem. Phys.*, 2011, **134**, 074706.
35 R. R. Netz, *J. Phys.: Condens. Matter*, 2003, **15**, S239.
36 A. Parsegian, *Nature*, 1969, **221**, 844–846.
37 J. N. Aqua, S. Banerjee and M. E. Fisher, *Phys. Rev. E: Stat., Nonlinear, Soft Matter Phys.*, 2005, **72**, 041501.
38 G. S. Manning and J. Ray, *J. Biomol. Struct. Dyn.*, 1998, **16**, 461–476.
39 R. A. Robinson and R. H. Stokes, *Electrolyte Solutions*, Dover Pubns, 2002.
40 A. Y. Grosberg, T. T. Nguyen and B. I. Shklovskii, *Rev. Mod. Phys.*, 2002, **74**, 329.

41 H. Boroudjerdi, Y.-W. Kim, A. Naji, R. R. Netz, X. Schlagberger and A. Serr, *Phys. Rep.*, 2005, **416**, 129–199.
42 D. Gillespie, *Nano Lett.*, 2012, **12**, 1410–1416.
43 J.-F. Pietschmann, M.-T. Wolfram, M. Burger, C. Trautmann, G. Nguyen, M. Pevarnik, V. Bayer and Z. Siwy, *Phys. Chem. Chem. Phys.*, 2013, **15**, 16917–16926.
44 E. Secchi, A. Niguès, L. Jubin, A. Siria and L. Bocquet, *Phys. Rev. Lett.*, 2016, **116**, 154501.
45 O. Coronell, M. I. González, B. J. Mariñas and D. G. Cahill, *Environ. Sci. Technol.*, 2010, **44**, 6808–6814.
46 S. Bason, Y. Oren and V. Freger, *J. Membr. Sci.*, 2011, **367**, 119–126.
47 N. Fridman-Bishop and V. Freger, *J. Membr. Sci.*, 2017, **540**, 120–128.
48 O. Nir, N. F. Bishop, O. Lahav and V. Freger, *Water Res.*, 2015, **87**, 328–335.
49 K. N. Kudin and R. Car, *J. Am. Chem. Soc.*, 2008, **130**, 3915–3919.
50 A. Tiraferri, N. Y. Yip, A. P. Straub, S. R.-V. Castrillon and M. Elimelech, *J. Membr. Sci.*, 2013, **444**, 523–538.
51 T. Y. Cath, A. E. Childress and M. Elimelech, *J. Membr. Sci.*, 2006, **281**, 70–87.
52 K. Spiegler, *Desalination*, 1971, **9**, 367–385.
53 E. Gileadi, *Electrode Kinetics for Chemists, Chemical Engineers, and Material Scientists*, VCH, New York, 1993.
54 E. L. Cussler, *Diffusion: mass transfer in fluid systems*, Cambridge university press, 2009.
55 A. S. Verkman, *Curr. Biol.*, 2013, **23**, R52–R55.
56 V. Freger, *Science*, 2015, **348**, 1317–1318.

 